Available online at www.sciencedirect.com
ScienceDirect
Journal of Nuclear Materials 362 (2007) 336–342
journal of nuclear materials
www.elsevier.com/locate/jnucmat

Processing of magnesia–pyrochlore composites for inert matrix materials

S.J. Yates [a,*], P. Xu [a], J. Wang [b], J.S. Tulenko [b], J.C. Nino [a]

[a] Department of Materials Science and Engineering, University of Florida, Gainesville, FL 32611, USA
[b] Department of Nuclear and Radiological Engineering, University of Florida, Gainesville, FL 32611, USA

Abstract

Inert matrix (IM) materials for nuclear fuel in light water reactors must meet several critical requirements that include high temperature stability, good irradiation behaviour, high thermal conductivity, and hot water corrosion resistance. MgO possesses all of the necessary requirements for an ideal IM candidate, except hot water corrosion resistance. A composite approach is being investigated in order to improve the corrosion resistance of MgO, while simultaneously taking advantage of the high thermal conductivity of MgO and its ability to be reprocessed in nitric acid. MgO–pyrochlore composite compositions are fabricated based on neutronic property simulations for assessment as potential IM materials. The selected pyrochlore compositions are synthesized by both sol gel and solid state processing, and how composite processing affects the microstructure will be discussed. Among the multiple composite processing approaches investigated, ball milling produces the most homogeneous and consistent microstructures.

PACS: 28.52.Fa

1. Introduction

Inert matrix materials are proposed to be used as non-fertile matrices for the transmutation of commercial and weapons grade plutonium in light water reactors. Through the transmutation of plutonium in light water reactors, there exists the potential to reduce both the accessible inventory of weapons grade plutonium and dramatically reduce the quantity of radioactive waste that must be safely disposed from commercial reactors. Although mixed oxide fuel (MOX) is currently utilized in light water reactors to recycle plutonium, MOX is fertile fuel that creates plutonium, even as it transmutates the plutonium originally mixed into the fuel. In order to avoid generating more plutonium from uranium fuel, materials for non-fertile matrices are being investigated as possible inert matrix fuels (IMF) for light water reactors.

Viable IMF materials must meet certain critical requirements that include high temperature stability, good irradiation behaviour, high thermal conductivity, and hot water corrosion resistance. Yttria-stabilized zirconia (YSZ) has attracted the most attention due to its chemical and structural

* Corresponding author. Tel.: +1 352 846 3768; fax: +1 352 846 3355.
E-mail address: mantha@ufl.edu (S.J. Yates).

0022-3115/$ - see front matter © 2007 Elsevier B.V. All rights reserved.
doi:10.1016/j.jnucmat.2007.01.171

stability; but the low thermal conductivity and the difficulty reprocessing has limited the IM applications of YSZ in a fuel cycle that relies on a reprocessing strategy [1]. MgO is an ideal IM candidate due to its high thermal conductivity and its ability to be easily reprocessed, however, its hot water corrosion resistance is poor. MgO and ZrO_2 composites were synthesized in an attempt to capture the best characteristics of both components, and the resulting composites have shown to exhibit acceptable thermal conductivities of $\sim$4–6 $Wm^{-1} K^{-1}$ at 1273 K and adequate corrosion resistance [2].

Pyrochlores are step forward in the development of oxide compounds for IMF applications because the pyrochlore crystal structure permits a wide range of substitutions from the rare earth elements. Lutique et al. [3] as reported a calculated thermal conductivity of $\sim$6 $Wm^{-1} K^{-1}$ at 1273 K for 90 vol.% MgO–10 vol.% $Nd_2Zr_2O_7$ composites. Atomistic simulations also suggest that other rare-earth zirconate pyrochlores are expected to possess thermal conductivities 5–15% higher than $Nd_2Zr_2O_7$ [4]. Other simulations propose that there exists the potential to synthesize MgO–pyrochlore composites that exhibit higher radiation tolerances than previously reported [5]. To assess the feasibility of MgO–pyrochlore composites as IMF materials, this paper describes selected compositions that were synthesized and characterized to determine the effect of processing on the microstructure of MgO–pyrochlore composites. Neutronic properties were also calculated to determine the neutron multiplication factor as a function of burnup for various ratios of MgO and pyrochlore.

2. Experimental procedure

2.1. Synthesis of $Nd_2Zr_2O_7$

2.1.1. Solid state synthesis of $Nd_2Zr_2O_7$

Stoichiometric ratios of Nd_2O_3 (Alfa Aesar 99.9%) and ZrO_2 (Alfa Aesar 99.7%) were added to the YSZ milling media in a Teflon ball mill jar with 100 ml of deionized water and 3 ml of ammonium polyacrylate dispersant (Darvan 821 A). The slurry was milled for 72 h on the ball mill, and dried overnight in an oven at 393 K. The dried powder was subsequently ground with the porcelain mortar and pestle and sieved through the 212 μm mesh. The sieved powder was placed in an alumina crucible and calcined at 1623 K in air for 12 h. X-ray was then performed to confirm phase purity. After calcination, the $Nd_2Zr_2O_7$ was added again to the prepared media in the Teflon ball mill jar with 100 ml of deionized water and 3 ml of ammonium polyacrylate dispersant (Darvan 821 A). The slurry was milled for another 48 h on the ball mill, and dried overnight in an oven at 393 K. The dried powder was finally ground with the porcelain mortar and pestle and sieved through the 212 μm mesh.

2.1.2. Sol gel synthesis of $Nd_2Zr_2O_7$

A 1 M solution was prepared by dissolving 0.02 mol of $Nd(NO_3)_3 \cdot 6H_2O$ (99.9%, Alfa Aesar) in 20 ml Acetic acid (99+%, Alfa Aesar). The solution was stirred at 300 rpm and heated to 378 K to evaporate the water. To make the sol, the solution was allowed to cool to room temperature, Zirconium (IV) *n*-propoxide (70% w/w in *n*-propanol, Alfa Aesar) was added to the solution in an equimolar ratio, the solution was then stirred for 15 min, and finally 5 ml of deionized water was added. The sol was dried at 393 K in oven for 24 h to form a gel, and followed by calcination of the gel at 1473 K for 6 h to achieve $Nd_2Zr_2O_7$ formation.

2.2. Composite fabrication

2.2.1. Mortar and pestle fabrication of $MgO–Nd_2Zr_2O_7$composites

The appropriate ratios of MgO and $Nd_2Zr_2O_7$ were added to an alumina mortar and pestle and ground for 5 min to thoroughly combine. The mixed powder was then synthesized into pellets.

2.2.2. Water magnetic stirring fabrication of $MgO–Nd_2Zr_2O_7$ composites

The process involved adding the appropriate ratio of Magnesia and $Nd_2Zr_2O_7$ to a beaker filled with 200 ml of deionized water. The slurry was agitated in an ultrasonic bath for 3 min to break up any agglomerates. The powder was then stirred for 6 h at 200 rpm and dried in an oven at 393 K overnight. The dried powder was crushed, sieved, and synthesized into pellets.

2.2.3. Ball milled fabrication of $MgO–Nd_2Zr_2O_7$ composite

The appropriate ratios of MgO and $Nd_2Zr_2O_7$ were added to the YSZ milling media in a Teflon ball with 100 ml of acetone. The slurry was milled for 24 h, and the acetone was allowed to evaporate overnight. The dried powder was then ground with

the porcelain mortar and pestle and sieved through the 300 μm mesh. The sieved powder was placed in an alumina crucible and subsequently calcined at 1273 K in air for 5 h. X-ray was performed on the calcined powder to confirm phase purity. The calcined powder was then synthesized into pellets.

2.3. Pellet fabrication

In order to characterize the properties of the $Nd_2Zr_2O_7$ and MgO composites, cylindrical pellets were fabricated. The appropriate ratio of $Nd_2Zr_2O_7$ and MgO was combined with 2 wt% of binder (Celvol 103 Polyvinyl Alcohol) and ground with an alumina mortar and pestle until the powder sieved through a 300 μm mesh. The sieved powder was then dried in the 393 K oven for 5 min to evaporate the water. Approximately 0.25 g of the powder was added to a 9.5 mm punch and die-set cleaned with acetone, lubricated with 1% stearic acid, and pressed with 190 MPa on a Carver press. The pellet was removed from the die and examined for cracks and surface finish. A geometric green density was calculated, and the pellets that met or exceeded the 58% of theoretical density were sintered in air at 1823 K for 4 h. The sintered pellets were also checked for cracks and surface finish, and a geometric density was calculated.

The theoretical pellet density of 4.970 g cm^{-3} for the 50 vol.% MgO–50 vol.% $Nd_2Zr_2O_7$ composite was calculated by multiplying the volume ratio of the composite components to its respective calculated theoretical density and adding the products together.

2.4. Sample preparation for microstructure analysis

The sintered pellets were radially cut and polished to 0.03 μm with alumina and thermally etched at 1723 K for 30 min. The thermally etched pellets were mounted with silver paint on an aluminium SEM sample holder and coated with carbon to improve the conductivity of the pellet and eliminate charging the sample with the electron beam. The resulting grain structure was analyzed with scanning electron microscopy (JEOL 6335 F) to assess the microstructure and connectivity of the MgO and $Nd_2Zr_2O_7$ phases. The SEM was operated using the secondary electron detector, with an accelerating voltage of 15 kV, and a working distance of approximately 15 mm.

3. Results and discussion

3.1. Pyrochlore synthesis

The pyrochlore type $A_2B_2O_7$ is cubic, and possesses Fd3m symmetry with the larger A^{3+} atoms in 8-fold coordination at the 16d sites and the B^{4+} atoms are in 6-fold coordination at the 16c sites. There are two types of O^{2-} ions in the pyrochlore lattice, with the 48f oxygen in tetrahedral coordination with two A^{3+} and two B^{4+} atoms, and the 8b oxygen is in tetrahedral coordination with four A^{3+} atoms. There is also an unoccupied O^{2-} tetrahedral site at 8a that is surrounded by four B^{4+} atoms. The 48f oxygen positional parameter x shifts the shape of the coordination polyhedra of A^{3+} and B^{4+} ions from a cube of A^{3+} ions when $x = 0.375$, to an octahedra of B^{4+} ions when $x = 0.3125$, with most pyrochlores possessing x parameters ranging between the two values. The typical lattice parameter for pyrochlores is approximately 10 Å [6].

Calcination optimization was performed on the solid state $Nd_2Zr_2O_7$ to determine the most efficient temperature and time to achieve a pure pyrochlore phase. Samples of the milled Nd_2O_3 and ZrO_2 were calcined at 1573 K, 1623 K, 1673 K, and 1723 K for 12 h. Phase pure $Nd_2Zr_2O_7$ also resulted from calcination of the milled powders at 1723 K for 6 h. Phase pure pyrochlore was achieved at all temperatures except 1573 K, and a representative X-ray spectrum of the calcined $Nd_2Zr_2O_7$ is shown in Fig. 1 along with an X-ray spectrum from sol gel synthesized $Nd_2Zr_2O_7$. Calcination optimization

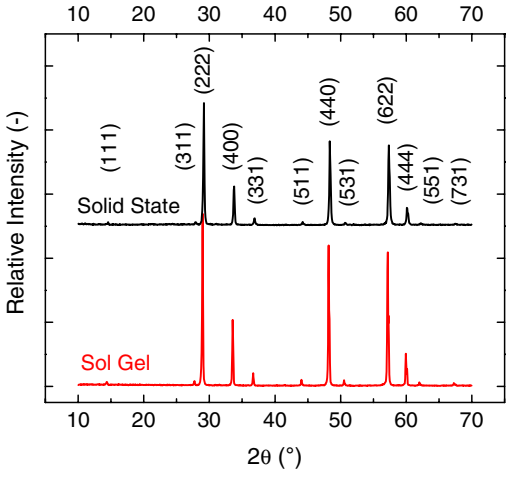

Fig. 1. XRD profile of solid state $Nd_2Zr_2O_7$ calcined at 1623 K and sol gel $Nd_2Zr_2O_7$ calcined at 1473 K.

for the sol gel $Nd_2Zr_2O_7$ was performed at 1273 K, 1423 K, and 1473 K for 6 h. Phase pure $Nd_2Zr_2O_7$ formed at 1473K for 6 h, 523 K lower than the solid state $Nd_2Zr_2O_7$ calcined for the same length of time.

The lattice parameter of the pyrochlore was determined using the Nelson–Riley function [7]. The Nelson–Riley function is computed in two parts by transforming the generated 2θ values and the corresponding diffraction planes from the X-ray pattern and performing the following calculations:

$$a(\theta) = \frac{\lambda\sqrt{(h^2+k^2+l^2)}}{2\sin(\theta)}, \quad (1)$$

$$a = a_0 - b\left(\frac{\cos^2(\theta)}{\sin(\theta)} + \frac{\cos^2(\theta)}{\theta}\right), \quad (2)$$

where θ is the X-ray phase angle in radians, λ is the X-ray wavelength of 1.54056 Å, and (hkl) are the indices of the diffraction peak corresponding to the angle θ. Both calculations are performed for each diffraction peak and the results are plotted as a vs. $f(\theta)$ in Fig. 2. Lattice parameter calculations using the Nelson–Riley function give a lattice parameter of 10.678 ± 0.002 Å and a theoretical density of 6.360 ± 0.001 g cm^{-3}. The lattice parameter and the corresponding theoretical density is similar to the data provided by Subramanian et al. [6], and close to the experimental data generated by Lutique et al. [3] for $Nd_2Zr_2O_7$.

Particle size characterization using laser light scattering (Beckman Coulter LS 13320) was performed on the powder to assess the average particle size and particle distribution of the $Nd_2Zr_2O_7$. The calcined $Nd_2Zr_2O_7$ was suspended in deionized water and placed in an ultrasonic bath for 30 s before adding it into the Beckman Coulter for analysis. The sonication is used to disperse the powder in the water by separating any weakly bonded agglomerates. A Fraunhofer model was selected to analyze the particles since the particles were expected to be larger than 1 μm. If the particle size distributions shown in Fig. 3 of the calcined powder and the calcined powder after ball milling for 48 h are compared, it is confirmed that the ball milling process after calcination reduces the powder from a bimodal particle distribution and an average particle size of 20 μm to the final particle size and distribution. The 48 h post calcination ball milling yielded a monodisperse particle distribution with an average particle size of 3 μm.

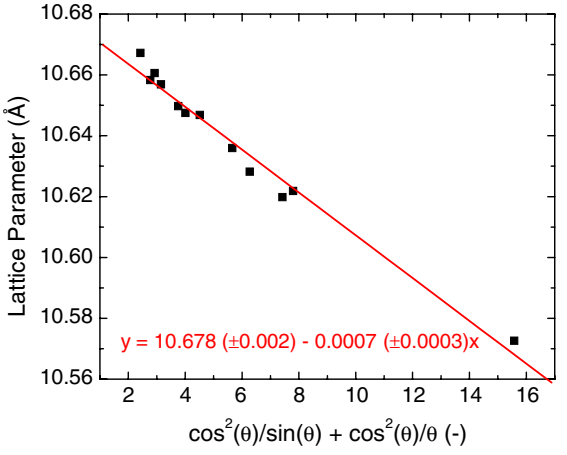

Fig. 2. Lattice parameter calculation for $Nd_2Zr_2O_7$.

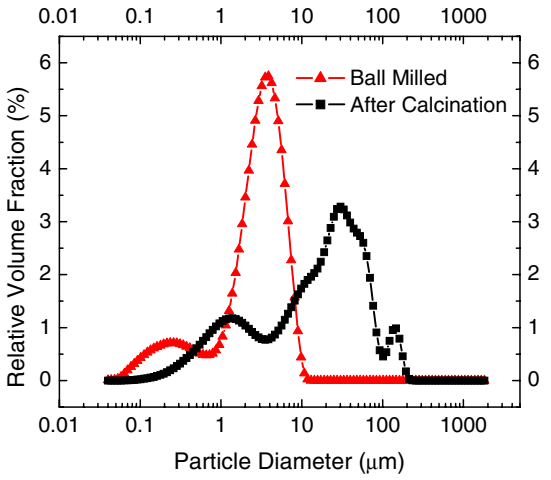

Fig. 3. Particle size and distribution of the calcined solid state synthesized $Nd_2Zr_2O_7$ and after the calcined solid state synthesized $Nd_2Zr_2O_7$ was ball milled for 48 h.

3.2. Neutronic property simulations

The inert matrix fuel burnup calculations were performed using Monteburns, a code that links the Monte Carlo transport code MCNP with the burnup and depletion code ORIGEN2. The simulations were based on a Framatome Mark-B 15X15 assembly design. Monte Carlo Neutron Photon Transport Code (MCNP) is a neutral particle transport code that uses Monte Carlo techniques, or a statistical method in which system characteristics are estimated by multiple computer simulations of the behaviour of individual particles within the system. ORIGEN2 computes decay and isotope depletion information for materials under irradiation.

MONTEBURNS couples the MCNP and ORIGEN2 packages to generate depletion and burn up calculations. CASMO is a multi-group, two-dimensional transport theory code for burn up calculations on BWR and PWR assemblies or simple pin cells. The results from the CASMO and MONTEBURNS models are compared when possible to ensure consistency and accuracy.

The MONTEBURNS [8] and MCNP [9] calculations were calculated using 50 burnup steps for 2000 full power days, or 60 $MWdkg^{-1}$ equivalent burnup. Because of the lack of neutron cross section data in the MCNP data library, ^{148}Nd was used as a replacement for ^{142}Nd, ^{144}Nd, ^{146}Nd, and ^{150}Nd [10]. The fissile material used in the calculations for both the IMF and MOX compositions was 8 vol.% weapons grade PuO_2. Different $Nd_2Zr_2O_7$–MgO volume ratios of 1:9, 3:7, and 5:5 were compared in the calculations to find the optimum result. The results in Fig. 4 show that the neutron multiplication factor, k_{eff}, of the IMFs are higher than MOX at the beginning of life (BOL) because of the neutron resonance absorption in the ^{238}U. The k_{eff} of the IMFs are lower than MOX at the end of life (EOL) because Pu is generated by neutron absorption in the ^{238}U. The k_{eff} also decreases with increasing amount of $Nd_2Zr_2O_7$ because the thermal neutron absorption cross-section of natural Nd is larger than that of natural Mg. The calculations show that the IMF composition with the $Nd_2Zr_2O_7$/MgO ratio of 3:7 is the best composite composition since it can provide enough EOL reactivity.

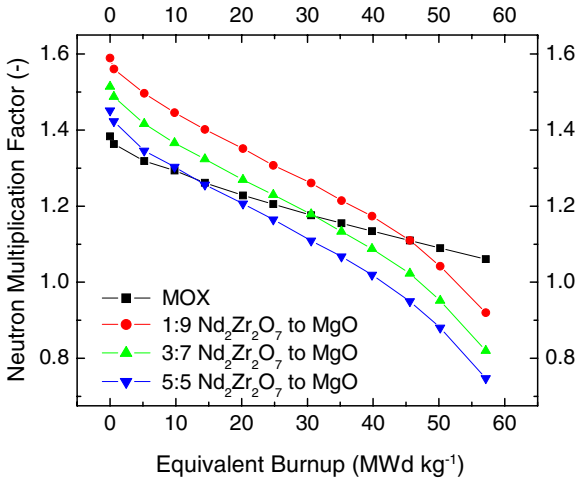

Fig. 4. Equivalent burnup data for $Nd_2Zr_2O_7$–MgO composite fuel compositions containing 8 vol.% weapons grade PuO_2.

3.3. Microstructure characterization of the Magnesia-$Nd_2Zr_2O_7$ composites

SEM analysis on the composites was performed to assess the microstructure, particularly focusing on the distribution of the MgO and $Nd_2Zr_2O_7$ phases and the interface between grains and between the phases. Since the secondary electron detector was used in the analysis, the dark grains on the SEM are MgO and the light grains are $Nd_2Zr_2O_7$, since the $Nd_2Zr_2O_7$ has a higher atomic weight than MgO.

As shown in Fig. 5(a), the microstructure throughout the mortar and pestle mixed pellets is characterized by agglomerates of MgO and $Nd_2Zr_2O_7$ surrounded by an interconnecting matrix of MgO and $Nd_2Zr_2O_7$ grains. The large agglomerates of MgO are detrimental to the corrosion resistance of the composite, however, since the MgO agglomerates will hydrate, swell, and cause cracks to form within the pellet eventually causing catastrophic failure [11]. This process also does not produce consistent microstructures, with different batches producing different agglomerate phases, sizes, and distributions. The inconsistent microstructures may also adversely affect the consistency of the thermal conductivity values, since the wide range of agglomerate sizes and distributions could affect the thermal conductivity data differently [12,13].

The microstructure from the magnetic water stirring process is shown in Fig. 5(b), and is characterized by a continuous $Nd_2Zr_2O_7$ phase with isolated agglomerates of MgO. This microstructure is consistent throughout multiple batches, with minor differences in the size and distribution of the agglomerates. The lack of a continuous MgO phase may reduce the thermal conductivity of the composite since there is not a thermally conductive path of MgO through the material [14]. While the continuous $Nd_2Zr_2O_7$ phase may provide better corrosion resistance, hydration and swelling of the large MgO agglomerates as hot water hydrates the grain boundaries of the MgO in the composite could cause the eventual catastrophic failure of the composite.

The microstructure of the pellets ball milled from the solid state $Nd_2Zr_2O_7$ is shown in Fig. 5(c) shows a completely homogeneous microstructure with a continuous connectivity of the $Nd_2Zr_2O_7$ phase. This microstructure is highly consistent, with no discernable differences in the microstructure between multiple batches of material. The observed

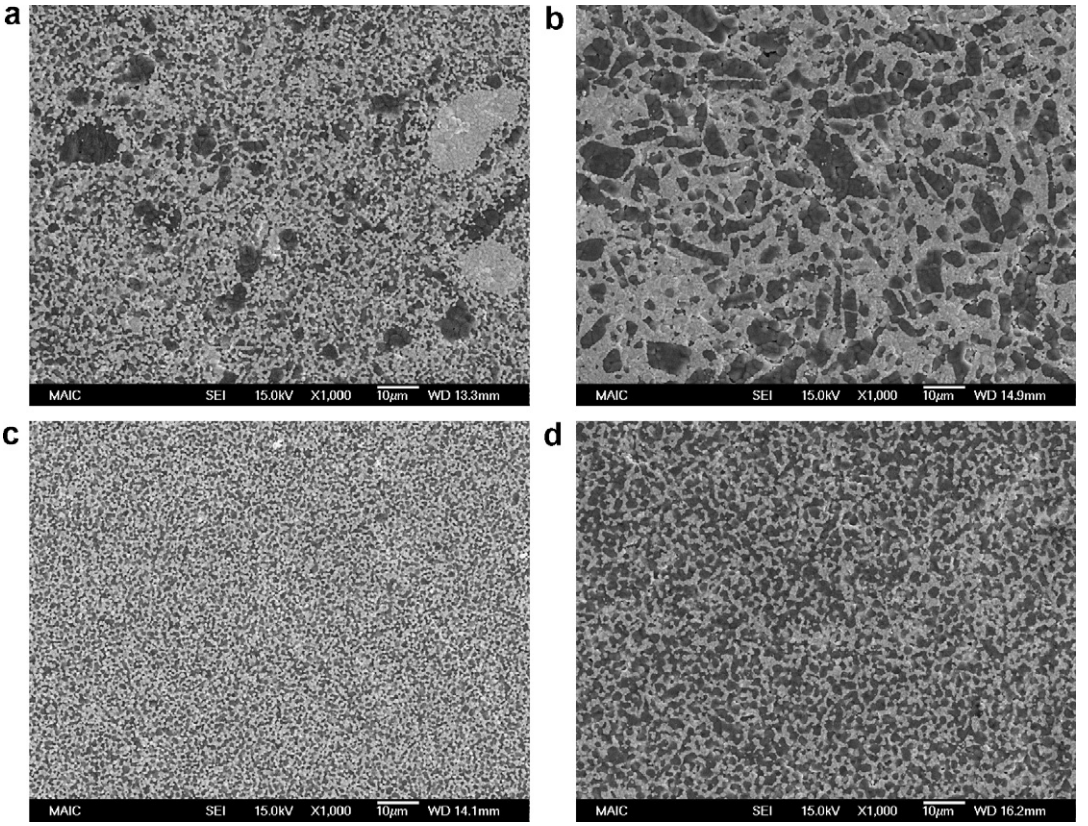

Fig. 5. SEM image of 50 vol.% MgO composite where the dark grains are MgO and the light grains are $Nd_2Zr_2O_7$. (a) Mortar and pestle mixing, (b) water magnetic stirring synthesis, (c) ball milled solid state $Nd_2Zr_2O_7$, (d) ball milled sol gel $Nd_2Zr_2O_7$.

connectivity of the pyrochlore phase will not adversely lower the thermal conductivity of the composite. However, the homogeneous microstructure may provide the maximum resistance to hot water corrosion based on the mechanism proposed by Kitamura et al. [15]. Previous work on MgO–ZrO_2 composites has shown that a continuous $Nd_2Zr_2O_7$ phase will provide a barrier to slow the hydration of MgO grain boundaries [16].

The final grain size of the MgO and $Nd_2Zr_2O_7$ is approximately 1 μm, potentially lowering the thermal conductivity due to the grain boundaries. The grain size decreases from the initial particle size of 3 μm because the $Nd_2Zr_2O_7$ and MgO is ball milled for another 24 h to mix the phases, further crushing the $Nd_2Zr_2O_7$ and MgO to the final grain size of 1 μm. Future work will focus on increasing the final grain size of the MgO and $Nd_2Zr_2O_7$ through modifications to the ball milling process to maintain the scale of mixing while reducing the ability of the ball mill to crush the particles.

Although MgO and $Nd_2Zr_2O_7$ shown in Fig. 5(c) is ball milled in acetone to reduce the potential to hydrate the MgO, Fig. 6 confirms the lack of MgO peaks after the two powders were mixed. This can possibly be attributed to the formation of $Mg(OH)_2$ on the surface of the MgO by hydrated acetone, or residual moisture from the ball mill jar and from the atmosphere [17]. A second calcination after ball milling at 1273 K for 5 h resulted in the reappearance of the MgO peaks, and the powder was then synthesized into pellets. X-ray was also performed on the sintered pellet to confirm that $Nd_2Zr_2O_7$ and MgO did not react and form new phases during sintering.

The pellets synthesized from ball milled sol gel $Nd_2Zr_2O_7$ shown in Fig. 5(d) also exhibits a homogeneous microstructure with continuous connectivity of the $Nd_2Zr_2O_7$ phase. The microstructure is also consistent between multiple ball milled batches of material, with little discernable differences in the microstructure. The final grain size of the sol gel $Nd_2Zr_2O_7$ is also comparable to the solid

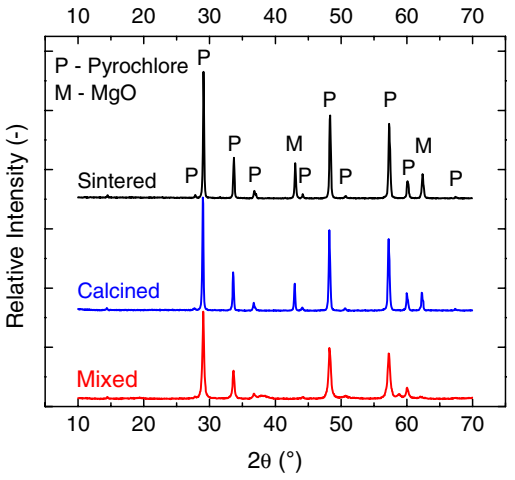

Fig. 6. XRD profiles of mixed, calcined, and sintered MgO–$Nd_2Zr_2O_7$ showing the disappearance of the MgO phase after mixing, the reappearance of the MgO after calcination, and the MgO and $Nd_2Zr_2O_7$ phases after sintering.

state $Nd_2Zr_2O_7$, with an average grain size of 1 μm. This may be due to a high sintering temperature of 1823 K and sintering time of 4 h, which may excessively coarsen the $Nd_2Zr_2O_7$ from its initial nanometer particle size [18]. Future work will also attempt to decrease the sintering time and temperature to minimize the degree of grain coarsening. The grain size of the MgO, however, averages 2–3 μm. The coarser MgO may enhance the thermal conductivity of the sol gel $Nd_2Zr_2O_7$ pellets, since the grain size of the thermally conductive MgO is maximized compared to that of the less thermally conductive $Nd_2Zr_2O_7$.

4. Conclusions

An MgO–$Nd_2Zr_2O_7$ composite has been investigated as a potential inert matrix for light water reactors. Several synthesis methods and composite processing routes were investigated. It was found that wet ball-milling mixing process produced the most homogenous and consistent microstructure. The observed connectivity between the MgO and $Nd_2Zr_2O_7$ grains is expected to enhance the thermal conductivity of the composite, while maximizing its corrosion resistance. A desirable grain size difference between the MgO (larger) and $Nd_2Zr_2O_7$-phases within the sintered composite was obtained utilizing sol-gel synthesized pyrochlore powders. This size difference is also expected to increase the thermal conductivity and corrosion resistance of the composite. However, experimental confirmation through high temperature thermal conductivity measurements is required. Neutronic property simulations on the IMF based on a MgO–$Nd_2Zr_2O_7$ inert matrix revealed the need for compositional variations to lower the initial neutron multiplication factor.

Acknowledgements

The authors would like to thank the Department of Energy for their support of this project under the Nuclear Energy Research Initiative (NERI) award DE-FC07-051D14647.

References

[1] C. Degueldre, T. Yamashita, J. Nucl. Mater. 319 (2003) 1.
[2] P.G. Medvedev, M.J. Lambregts, M.K. Meyer, J. Nucl. Mater. 349 (2006) 167.
[3] S. Lutique, R.J.M. Konings, V.V. Rondinella, J. Somers, T. Wiss, J. Alloys Compd. 352 (2003) 1.
[4] P.K. Schelling, S.R. Phillpot, R.W. Grimes, Philos. Mag. Lett. 84 (2004) 127.
[5] K.E. Sickafus, L. Minervini, R.W. Grimes, J.A. Valdez, M. Ishimaru, F. Li, K.J. McClellan, T. Hartmann, Science 289 (2000) 748.
[6] M.A. Subramanian, G. Aravamundan, G.V. Suba Rao, Prog. Solid State Chem. 15 (1983) 55.
[7] B.D. Cullity, S.R. Stock, Elements of X-Ray Diffraction, third Ed., Prentice Hall, New Jersey, 2001.
[8] MONTEBURNS Burnup Code System, Version 2.0, Los Alamos National Laboratory, PSR-455.
[9] MCNP Burnup Code System, Version 2.0, Los Alamos National Laboratory, LA-CP-02-408.
[10] H. Etherington, Nuclear Engineering Handbook, McGraw Hill, Columbus, OH, 1958.
[11] E.A.C. Neeft, K. Bakker, R.L. Belvroy, W.J. Tams, R.P.C. Schram, R. Conrad, A. van Veen, J. Nucl. Mater. 317 (2003) 217.
[12] K. Bakker, R.J.M. Konings, J. Alloys Compd. 271–273 (1998) 632.
[13] J.K. Carson, S.J. Lovatt, D.J. Tanner, A.C. Cleland, Int. J. Refrig. 26 (2003) 873.
[14] L. Berlyand, V. Mityuchev, J. Stat. Phys. 118 (2005) 481.
[15] A. Kitamura, K. Onizuka, K. Tanaka, Taikabutsu Overseas. 16 (1996) 112.
[16] P.G. Medvedev, S.M. Frank, T.P. O'Holleran, M.K. Meyer, J. Nucl. Mater. 342 (2005) 48.
[17] O. Fruhwirth, G.W. Herzog, I. Hollerer, A. Rachetti, Surface Tech. 24 (1985) 301.
[18] M.W. Barsoum, Fundamentals of Ceramics, Institute of Physics, Bristol, England, 2003.